

شبكة المعلومات الجامعية التوثيق الإلكتروني والميكروفيلو

# بسم الله الرحمن الرحيم





MONA MAGHRABY



شبكة المعلومات الجامعية التوثيق الإلكتروني والميكروفيلو



شبكة المعلومات الجامعية التوثيق الالكتروني والميكروفيلم



MONA MAGHRABY



شبكة المعلومات الجامعية التوثيق الإلكترونى والميكروفيلم

## جامعة عين شمس التوثيق الإلكتروني والميكروفيلم قسم

نقسم بالله العظيم أن المادة التي تم توثيقها وتسجيلها علي هذه الأقراص المدمجة قد أعدت دون أية تغيرات

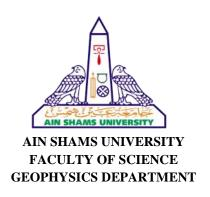


يجب أن

تحفظ هذه الأقراص المدمجة بعيدا عن الغبار



MONA MAGHRABY





### Mineralization Significance of Airborne Gamma Ray Spectrometric and Magnetic Data of Gabal Umm Naggat Area, Central Eastern Desert, Egypt

A Thesis Submitted in Partial Fulfillment of the Requirement for The Degree of Master Science (M.Sc.) in Geophysics

By

Salem Othman Mustafa Bourgieaa

To

Geophysics Department
Faculty of Science
Ain Shams University

Supervised by

#### Prof. Dr. Sami Hamed Abd El-Nabi

Professor of Geophysics

Geophysics Department – Faculty of Science Ain Shams University – Cairo – Egypt

#### Ass. Prof. Karam Samir Ibrahim Farag

Associate Professor of Geophysics

Geophysics Department – Faculty of Science Ain

Shams University – Cairo – Egypt

#### **ACKNOWLEDGEMENT**

With the aid and inspiration of Allah that guided and strengthened me, this dissertation was completed. I would like to express my gratitude to all those who have helped me in the last few years, but some people deserve special thanks.

First of all, I would like to thank my supervisors **Prof. Dr. Sami Hamed Abd El-Nabi**, Professor of Geophysics, Head of Petroleum Geophysics Program, Faculty of Science, Ain Shams University, for his guidance and great help in making this work perfect. Special thanks to **Dr. Karam Samir Farag**, Associate professor of Geophysics, Geophysics Department, Faculty of Science, Ain Shams University, for his help and support.

Finally, I would like to express my deepest gratitude and warm thanks to my wife for her support, encourage and patience in this journey which was really the main driving force for me not only to complete this work but also to live.

My Mother, all my family members and everyone else believed that I could do something good, deserve special thanks for their support in this last very tiring period. It feels good to know that they are always ready to help.

Salem Othman Mustafa Bourgieaa

#### **ABSTRACT**

The area under study lies in the Central Eastern Desert of Egypt. It covers about 1417 Km<sup>2</sup> in surface area and is located between Lat. 25° 10′ 48″ and 25° 32′ 56″ N and Long. 33° 56′ 27″ and 34° 18′ 7″ E.

The study area is characterized by both gentle and rough topography. It is traversed by many wadis (dry valleys) as W. EL Miyah, W. Umm Gheig, W. Umm Bisilla and W. El Jundi. The topographic values range from 404-1286 meters. The study area is primarily occupied by basement rocks that include various volcano-sedimentary rock associations and ophiolitic mafic-ultramafic rock associations. Quaternary sediments in the mapped area represented by wadi sediments are composed of detritus, sands, pebbles and rare boulders that are generally created by weathering of previously-existing basement rocks. The general structural setting of the area under investigation could be summarized to dominant trends of surface structural lineament in two main trends ENE-WSW and NNW-SSE and miner trends in NE-SW and NW-SE directions.

The radiometric gamma ray spectrometric data are in the forms of total counts (TC) in unit of (Ur), potassium (K) in (%), equivalent uranium (eU) and equivalent thorium (eTh) in (ppm). In addition of the ratios of eU/eTh, eU/K and eTh/K, these seven variables are then gridded, colored, and contoured for better qualitative interpretation of the radioelement distributions through the different surface exposed rock units. Zonation maps of TC, eU, eTh and 3D view of TC clearly demonstrate the contact and dimensions of alteration zone of albite granite of Umm Naggat pluton in terms of radiometric point of view. TC values range is from 28.3 to 75 in Ur, eU values range is from 11 to 38.1 ppm and eTh values range from 29 to 56 ppm and the dimensions is represented by two locality on oval shape. Both locality has E-W direction. Albite granite anomalous zone it could be considered as a primary target.

Factor analysis technique are used for carrying out the quantitative interpretation, with seven variables of TC, eU, eTh, K%, eU/eTh, eU/K and eTh/K to generate three factors F1, F2, F3, where those factors could facilitate the spatial correlation of features in the various data sets, and at the same time displayed variations which difficult to be determined. These factor scores are multiplied by 100 and then gridded, colored and contoured. Factor1

can be identified as the factor of integrated radioactivity or factor of uranium exploration. Factore2 used to different the rock type. Factor 3 refers to rock basicity.

Outlining uraniferous provinces zones was carried out in three ways according to Saunders and Potts (1976). Way one by compare the average of each rock unit with the published crustal average value. Way two construct point anomaly map and way three examining profiling over anomalous zones. The first way of defining anomalies is by calculating the average uranium values for each of the various rock units and comparing them with the published crustal average value for each rock type involved to find uraniumenriched units. A comparison of the calculated uranium average for each rock unit with its corresponding crustal average shows that the younger granites of the three plutons Umm Naggat, Umm Bisilla and El Unayji have uranium a values exceed the crustal average of acidic rocks. Second way in outlining the uraniferous anomalous zone based on calculation for properties where their data differ significantly from the mean background of the data. The high anomalous values are considered as the values equaling or exceeding at least two standard deviations from the calculated arithmetic mean values (X+2S) & (X+3S) for eU measurements, for a single point in each rock unit. This acceptable technique was chosen for distinguishing between the normal and abnormal measurements, which could be considered as anomalous values according to (Saunders & Potts, 1976) technique for calculating the significant factor of each gamma-ray spectrometric variable in each rock unit. Thirdly, stacked profiles construction along selected flight lines for outlined uranium anomaly enrichment in order to facilitate the follow up of the response of anomalous zones on the different spectrometric channels plus the topographic channel. These profiles have been shown in flight lines, L2390, L2400, L2570, L2580, L2600, and L2610. Most of these lines show high eU, eU/eTh and eU/K channels. The result of these three ways highlight to the location of three anomalous zones. These anomalies are considered to represent the first priority for ground follow-up. It was evident throughout this work that, most of the identified gamma-ray spectrometric anomalies was found to be closely related to the surface faulting directions prevailing in the region.

The airborne magnetic data obtained from the survey over the mapped area has been analyzed by various techniques such as the reduction to the north magnetic pole (RTP), isolation of the regional and residual magnetic components using Gaussian filtering technique, calculation of the magnetic depth calculation. Three techniques of magnetic depth

calculation as the Source Parameter Image (SPI), Analytic Signal (AS) and Euler Deconvolution were applied. The deduced depth maps show that results are much closed to each other. The integration of all these techniques has been resulted in the construction of the interpreted magnetic basement tectonic map for the study area.

The constructed tectonic basement map shows that deep-seated structure of the study area oriented in NNW (Atalla trend) and WNW (Najd trend) as primary trends while the ENE to nearly E-W ranked as secondary trend, while the near surface structure of the study area oriented in NNW (Atalla trend) and N-S (East-African) as primary while the NE (Trans-African) to nearly NNE (Agaba) ranked as secondary trend.

### **Table of Content**

ACKNOWLEDGEMENT	I
ABSTRACT	II
Table of Content	V
List of Figures	IX
List of Tables	XII
<b>CHAPTER 1:INTRODUCTION</b>	
1.1. Location	1
1.2. Topography	1
1.3. Aim of the Study	2
1.4. Previous Work	4
CHAPTER 2:GEOLOGICAL SETTING	
2.1.General	
2.2. Litho-Stratigraphic Succession of the Surveyed Area	
2.2.1.1.Serpentinites (SP)	
2.2.1.2.Metagabbro-Diorite Complex (mg&mgi)	
2.2.1.3.Metavolcanics	
2.2.1.4.Metasediments (ms)	
2.2.1.5.Hammamat Sediments (ha)	
2.2.1.6.Older Granitoids (Grey Granite -gα)	
2.2.1.7. Younger Granitoids (Pink Granite $-g\beta\&\ g\gamma$ )	
2.2.1.8.Trachyte Plugs (TR)	
2.2.2.1.Sedimentry Deposits (Quaternary)	
2.3.Minerlazaions	
2.3.1.Umm Naggat Mineral Occurrence	16
2.3.2. Umm Samra-Umm Bakra Vein-Type	
2.3.3.BIF of Gabal AL Hadid	
2.3.4. Umm Bisilla Quartz Veins	18
2.3.5. Magnesite	18
2.3.6.Fluorite	18
2.4 Structure Setting	19
2.4.1.General	_
2.4.2. Trend Pattern	19
2.4.2.1.Trans-African trend (NE-SW)	20
2.4.2.2 Atalla trand (NNW SSE)	20

2.4.2.3.Gulf of Suez - Red sea trend (NW-SE)	20
2.4.2.4.Meridional or east African trend (N-S)	21
2.4.2.5.Gulf of Aqaba trend (NNE-SSW)	
2.4.2.6.Najd trend (WNW-ESE)	21
CHAPTER 3:AIRBORNE GEOPHYSICAL DATA AC	CQUISITION
AND PROCESSING	
3.1. General	
3.2. Data Acquisition	
3.3. Spectrometric Survey	
3.3.1. Principle of Radioactivity	
3.3.1.1. Types of Radioactive Decay	
3.3.1.2. Natural Sources of Radiation	
3.3.1.3. Disequilibrium	27
3.3.1.4. Interaction of Gamma Rays with Matter	
3.3.1.5. Attenuation of Gamma-Ray Flux with Height	28
3.3.1.6. Altitude Attenuation Coefficients or STP Calculation	
3.3.2.Radiometric Survey Method	
3.3.3.Background Radiation	
3.3.3.1.Cosmic Rays	
3.3.3.2.Atmospheric Radioactivity Source	
3.3.3.Radioactivity of the Measuring System	
3.3.4.Instrumentation	
3.3.4.1.Aircraft	33
3.3.4.2.Radar Altimeter	
3.3.4.3.Voltage-to-Frequency Converter	
3.3.4.4.Gamma-Ray Spectrometer	
3.3.4.5.Detector Interface	
3.3.4.6.Analog-to-Digital Converter	
3.3.4.7.Analog Recording	
3.3.4.8.Temperature Sensor	
3.3.5.Instrument Calibration	
3.3.6.Navigation System	
3.3.6.1.Path Recovery Camera	
3.3.6.2.Doppler Navigation System	
3.3.7.Pre-Processing	
3.3.8. Processing	
3.3.8.1. Dead Time Correction	
3.3.8.2 Energy Calibration	
3.3.8.3. Cosmic and Aircraft Background Removal	40
3.3.8.4. Radon Background Removal	41

3.3.8.5. Stripping Correction	41
3.3.8.6. Height Correction	41
3.3.8.7. Conversion to Elemental Concentrations	41
3.4. Aeromagnetic Survey	42
3.4.1.General	42
3.4.2. Magnetic Properties of Rocks	42
3.4.3. Airborne Magnetometer	43
3.4.4. Base Station Magnetometer	44
3.4.5. Recording System	44
3.4.6. Airborne Magnetic Data Processing	44
3.4.6.1.Edit	44
3.4.6.2. Diurnal Correction	45
3.4.6.3. Heading Correction	45
3.4.6.4. Parallax / Lag Correction	45
3.4.6.5. International Geomagnetic Reference Field (IGRF)	46
3.4.6.6.Magnetic Adjustment (Leveling)	46
3.4.6.7.Tie-Line Leveling	46
4.1 General 4.2 Interpretation of Airborne Gamma-ray Spectrometric Data	_
4.2 Interpretation of Airborne Gamma-ray Spectrometric Data	
4.2.1 Qualitative Interpretation of Aero-Spectrometric Maps	
4.2.1.1 Total-count (TC) Contour Map	
4.2.1.2 Potassium (K%) Contour Map	
4.2.1.3 Equivalent Uranium (eU) Contour Map	
4.2.1.3 Equivalent Thorium (eTh) Contour	
4.2.1.4 Equivalent Uranium/Thorium (eU/eTh) Ratio Contour Map:	
4.2.1.5 Equivalent Uranium /Potassium (eU/K) Ratio Contour Map:	
4.2.1.6 Equivalent Thorium / Potassium (eTh/K) Ratio Contour Map:	
4.2.2 Ternary Composite Maps	
4.2.2.1 The Ternary Composite Maps:	
4.2.2.2 Potassium Composite Map	
4.2.2.3 Equivalent Uranium Composite Map	
4.2.2.4 Equivalent Thorium Composite Map	
4.2.2 Quantitative Interpretation of Gamma-Ray Spectrometric Maps	
4.2.2.1 Factor Analysis Techniquei-Factor1:	
ii-Factor2:	
iii-Factor3:	
4.2.2.2 Outlining Uraniferous Provinces:	
I-The First Way:	

II-The Second Way:	
III-The Third Way	
4.3. Relation of Anomalous Zones and Topography	
4.4. Relation of Anomalous Zones and Fault Pattern	96
CHAPTR 5:INTERPRETATION OF MAGNETIC DATA	
5.1.General	99
5.2. Qualitative Interpretation	100
5.2.1.Total Intensity Magnetic Map	101
5.2.2. Removal of the Earth's Regional Gradient	103
	104
5.2.3.Reduction to the North Magnetic Pole	
5.2.4.Zonataion Map of RTP	107
5.2.4.1. Low Magnetic Zone (-974nT to -50nT)	107
5.2.4.2. Intermediate Magnetic Zone (-50nT to 80nT)	107
5.2.4.2. High Magnetic Zone (80nT to 2070nT)	107
5.2.4.The Energy (Power) Spectrum	109
5.2.4.Gaussian Regional / Residual Filter	111
5.2.5. Residual Magnetic Component Map	111
5.2.6. Regional Magnetic Component Map	112
5.3. Quantitative Interpretation of the Aeromagnetic Data	115
5.3.1. Magnetic Depth Calculations	115
5.3.1.1. Analytic Signal (AS)	115
5.3.1.2. Source Parameter Imaging (SPI) Technique	118
5.3.1.3. 3D Euler Deconvolution Method	120
5.3.2 Interpreted Magnetic Subsurface Structure Map	123
5.3.2.1.Tilt Derivative (TD)	
5.3.2.2. Horizontal Tilt Derivative (TDX)	126
5.3.2.3. Structural Interpretation	129
5.3.2.3.1.General	129
5.3.2.3.2.Deep Seated Structure map	130
5.3.2.3.3.Shallow Seated Structure map	132
CONCLUSION	135
REFERENCES	140
الملخص العربي	اً ۔۔۔۔۔۔اُ

## **List of Figures**

Figure No.	Title	Page
Fig.1.1	Location Map of the Study Area of G. Umm Naggat Area, Central	1
	Eastern Desert, Egypt	
Fig.1.2	Topography and Drainage Map of G. Umm Naggat Area, Central Eastern Desert, Egypt.	3
Fig.2.1	Geologic Map of Umm Naggat Area, Central Eastern Desert, Egypt (Modified After Conoco, 1987).	9
Fig.2.2	Mineralized Zone of Umm Samra-Umm Bakra at G. Umm Naggat Area, Central Eastern Desert, Egypt ( <b>After Ibrahim et al. 2017</b> ).	17
Fig.2.3	Azimuth Rose Diagram of The Structural Element Deduced from Geological Map of G. Umm Naggat Area, Central Eastern Desert, Egypt.	19
Fig.3.1	Index Map of The Airborne Magnetic and Gamma-Ray Spectrometric Survey of Area II, Block 71, G. Umm Naggat Area, Central Eastern Desert Egypt (after Aero Service 1984).	23
Fig.3.2	Flight Path Map of Airborne Magnetic and Gamma Ray Spectrometric Survey of G. Umm Naggat Area, Central Eastern Desert, Egypt (after Aero Service 1984).	25
Fig.3.3	The Interaction of Gamma Rays With Matter (after IAEA, 2003)	28
Fig.3.4	Variation in Count Rate With Flight Altitude (After IAEA, 2003)	30
Fig.3.5	Aircraft Used in the Study Area, Cessna Titan, Type 404	34
Fig.3.6	Standard Flow Chart for Gamma-Ray Spectrometric Data Processing (after IAEA1991)	39
Fig.3.7	Index Map of Aeromagnetic Data Block71 of G. Umm Naggat Area, Central Eastern Desert, Egypt (after Aero Service 1984).	46
Fig.4.1	Typical Gamma-Ray Spectrum of the Three Radioelements, Potassium, Uranium and Thorium with The Energy Windows Used to Detect Them (after IAEA, 1991).	48
Fig.4.2	Filled Color Total Count (TC) Contour Map of G. Umm Naggat Area, Central Eastern Desert, Egypt (after Aero Service 1984).	51
Fig.4.3	Visualized Five Zonal Area of Total Count (TC) Map of G. Umm Naggat Area, Central Eastern Desert, Egypt.	52
Fig.4.4	3D View of Total Count Map, of G. Umm Naggat Area, Central Eastern Desert, Egypt.	53
Fig.4.5	Filled Color Potassium (K%) Contour Map of G. Umm Naggat Area, Central Eastern Desert, Egypt (after Aero Service 1984).	55
Fig.4.6	Visualized Three Zonal Area of Potassium (K%) Map of G. Umm Naggat Area, Central Eastern Desert, Egypt.	56
Fig.4.7	Filled Color Equivalent Uranium (eU) Contour Map, of G. Umm Naggat Area, Central Eastern Desert, Egypt (after Aero Service 1984).	57
Fig.4.8	Visualized Four Zonal Area of Equivalent Uranium (eU) Map of G. Umm Naggat Area, Central Eastern Desert, Egypt.	58

Fig.4.9	Filled Color Equivalent Thorium (eTh) Contour Map of G. Umm	60
	Naggat Area, Central Eastern Desert, Egypt (after Aero Service	
	1984).	
Fig.4.10	Visualized Five Zonal Area of Equivalent Thorium (eTh) Map of G.	61
	Umm Naggat Area, Central Eastern Desert, Egypt.	
Fig.4.11	Filled Color (eU/eTh) ratio Contour Map of G. Umm Naggat Area,	63
	Central Eastern Desert, Egypt (after Aero Service 1984).	
Fig.4.12	Filled Color (eU/k) ratio Contour Map of G. Umm Naggat Area,	64
	Central Eastern Desert, Egypt (after Aero Service 1984).	
Fig.4.13	Filled Color (eTh/K) ratio Contour Map of G. Umm Naggat Area,	65
	Central Eastern Desert, Egypt (after Aero Service 1984).	
Fig.4.14	False Color Ternary Composite map, of G. Umm Naggat Area,	70
	Central Eastern Desert, Egypt.	
Fig.4.15	False Color Potassium Composite Map, of G. Umm Naggat, Area,	71
	Central Eastern Desert, Egypt.	
Fig.4.16	False Color Uranium Composite map, of G. Umm Naggat Area,	72
	Central Eastern Desert, Egypt.	
Fig.4.17	False Color Thorium Composite Map, of G. Umm Naggat Area,	73
	Central Eastern Desert, Egypt.	
Fig.4.18	Filled Color Factor (1) Contour of Map of G. Umm Naggat Area,	80
	Central Eastern Desert, Egypt.	
Fig.4.19	Filled Color Factor (2) Contour of Map of G. Umm Naggat Area,	81
	Central Eastern Desert, Egypt.	
Fig.4.20	Filled Color Factor (3) Contour of Map of G. Umm Naggat Area,	82
	Central Eastern Desert, Egypt.	
Fig.4.21	Representative Graph of Calculated Background Mean (X) of	84
	Radioelements, for The Different Rock Units of the Umm Naggat	
	Area, Central Eastern Desert, Egypt.	
Fig.4.22	The Uranium Point Anomaly Map, of G. Umm Naggat Area, Central	86
	Eastern Desert, Egypt	
Fig.4.23	Detailed Point Anomaly Map of Anomalous Enrichment of G. Umm	87
	Naggat Pluton, Central Eastern Desert, Egypt.	
Fig.4.24	Stacked Profile taken along Flight Line 2610 (After Aero Service,	90
	1984).	
Fig.4.25	Stacked Profile taken along Flight Line 2600 (After Aero Service,	91
T: 406	1984).	0.0
Fig.4.26	Stacked Profile taken along Flight Line 2570 (After Aero Service,	92
E' 4 25	1984).	02
Fig.4.27	Stacked Profile taken along Flight Line 2580 (After Aero Service,	93
E: ~ 4.20	1984). Stocked Duefile telephone Flight Line 2200 (After Acre Service	04
Fig.4.28	Stacked Profile taken along Flight Line 2390 (After Aero Service,	94
Fig 4 20	1984). Stacked Profile token along Elight Line 2400 (After Aero Service)	95
Fig.4.29	Stacked Profile taken along Flight Line 2400 ( <b>After Aero Service</b> , <b>1984</b> ).	73
Fig.4.30	Stream Order Superimposed On Point Anomaly Map of G. Umm	97
11g.4.30	Naggat Area, Central Eastern Desert, Egypt.	71
Fig.4.31	Fault Pattern Superimposed On Point Anomaly Map of G. Umm	98
1 1g.7.31	Naggat Area, Central Eastern Desert, Egypt.	70
1	i massaci moa, comi ai - Dastem Dosti, Egypt.	1

Fig.5.1	Total Intensity Aeromagnetic Map of G. Umm Naggat Area, Central	102
	Eastern Desert, Egypt (After Aero Service, 1984).	
Fig.5.2	Zero Levelled Total Intensity Aeromagnetic Map of G. Umm Naggat	104
	Area, Central Eastern Desert, Egypt (After Aero Service, 1984).	
Fig.5.3	Reduction to The North Pole (RTP)Aeromagnetic Intensity Map of G.	106
	Umm Naggat Area, Central Eastern Desert, Egypt (After Aero	
	Service, 1984).	
<b>Fig.5.4</b>	Zonation of RTP Magnetic Intensity Map of G. Umm Naggat Area,	108
	Central Eastern Desert, Egypt.	
Fig.5.5	Radially Averaged Power Spectrum and Depth Estimation of The	111
	RTP Aeromagnetic Intensity Map of G. Umm Naggat Area, Central	
	Eastern Desert, Egypt.	
Fig.5.6	Residual RTP Aeromagnetic Intensity Map of G. Umm Naggat Area,	113
	Central Eastern Desert, Egypt.	
Fig.5.7	Regional RTP Aeromagnetic Intensity Map of G. Umm Naggat	114
	Area, Central Eastern Desert, Egypt.	
<b>Fig.5.8</b>	Filled Color Analytical Signal Contour Map of The RTP Magnetic	117
	Intensity of G. Umm Naggat Area, Central Eastern Desert, Egypt.	
Fig.5.9	Filled Color Source Parameter Image Contour Map of The RTP	119
	Magnetic Intensity of G. Umm Naggat Area, Central Eastern Desert,	
	Egypt.	
Fig.5.10	3D Euler Deconvolution with SI (0) of The RTP Magnetic Intensity	122
	Map of G. Umm Naggat Area, Central Eastern Desert, Egypt.	
Fig.5.11	Tilt Derivative Map of the Regional of G. Umm Naggat Area, Central	124
	Eastern Desert, Egypt.	
Fig.5.12	Tilt Derivative Map of the Residual of G. Umm Naggat Area, Central	125
	Eastern Desert, Egypt.	
Fig.5.13	3D Euler Solution of Index (SI=0) superimposed on Residual Total	127
	Horizontal Tilt Derivative (THDR_TDR) map of G. Umm Naggat	
	Area, Central Eastern Desert, Egypt.	
Fig.5.14	3D Euler Solution of Index (SI=0) superimposed on Regional Total	128
	Horizontal Tilt Derivative (THDR_TDR) map of G. Umm Naggat	
	Area, Central Eastern Desert, Egypt.	
Fig.5.15	Interpreted Deep Seated Structure of G. Umm Naggat Area, Central	131
	Eastern Desert, Egypt.	
Fig.5.16	Azimuth Rose Diagram of Deep Seated Structure of G. Umm Naggat	132
	Area, Central Eastern Desert, Egypt.	4.5
Fig.5.17	Interpreted Shallow Seated Structure of G. Umm Naggat Area,	133
	Central Eastern Desert, Egypt.	
Fig.5.18	Azimuth Rose Diagram of Shallow Seated Structure of G. Umm	134
	Naggat Area, Central Eastern Desert, Egypt.	